1 **Appendix A. Supplementary data**

2 **Table S1.** The short name of synthesized samples with different synthesis condition

sample	condition				lable
	$NaWO_4 \cdot H_2O$(g)	$Pb(AC)_2 \cdot 3H_20$(g)	HNO_3(ml)	Ethylene glycol(ml)	
1	0.53	0	3	1	WO_3
2	0.53	0.0758	3	1	WP-1
3	0.53	0.1516	3	1	WP-2
4	0.53	0.2274	3	1	WP-3
5	0.53	0.3032	3	1	WP-4
6	0.53	0.3790	3	1	WP-5
7	0.53	0.4548	3	1	WP-6
8	0.53	0.62	3	1	$PbWO_4$

3 **Table S2.** XPS data of PW, PWH-5, and W

	O 1s	**W 4f**	**Pb 4f**	**VB**	**O**	**W**	**Pb**
	(eV)	**(eV)**	**(eV)**	**(eV)**	**(%)**	**(%)**	**(%)**
WO_3	**529[1].7**	**34.7**	-	**2.68**	**55.31**	**21.07**	-
		36.8					
WP-4	**529.7**	**34.7**	**138.1**	-	**49.31**	**15.14**	**4.73**
		36.8	**143.0**				
$PbWO_4$	**529.6**	**34.4**	**137.6**	**1.66**	**35.36**	**9.16**	**8.96**
		36.5	**142.4**				

4

5 **Table S3.** BET surface areas, pore volumes, and pore size of the samples

Samples	BET surface areas (m^2g^{-1})	Pore volume (cm^2g^{-1})	Pore size (nm)
WO_3	5.3826	0.022076	15.9904
WP-1	37.5730	0.235167	25.0357
WP-2	34.0102	0.185593	21.8279
WP-3	9.4986	0.093349	39.3107
WP-4	12.6849	0.087182	27.4916
WP-5	1.8648	0.011727	25.1536
WP-6	1.9938	0.026214	52.5989
$PbWO_4$	1.8770	0.016863	35.9362

6 **Table S4.**The corresponding report of WO_3, $PbWO_4$ and composite photocatalysts for RhB

7 degradation

Photocatalysts	RhB (mg/L)	Time (min)	Dosage	Light Source	Removeal efficiency (%)	Refs.
$WO_3/Ag/Ag_3PO_4$	20	120	100ml/100mg	UV filter 500 W Xe-lamp	92%	[2]
WO_3/MoS_2	10	120	100ml/50mg	500 W tungsten halogen lamp	98.2%	[3]
WO_3	4	150	100ml/30mg	UV filter 300 W Xe-lamp	99%	[4]
WO_3/Bi_2WO_6	5	150	10ml/10mg	UV filter 500 W Xe-lamp	78.1%	[5]
$PbWO_4$:9%Eu^{3+}	5	240	50ml/50mg	UV light 500 W mercury lamp	90.85%	[6]
$PbWO_4$	2.4	105	50ml/50mg	UV filter 500 W Xe-lamp	100%	[7]
WP-4	5	30	100ml/50mg	300 W Xe lamp	98.6%	This work

8

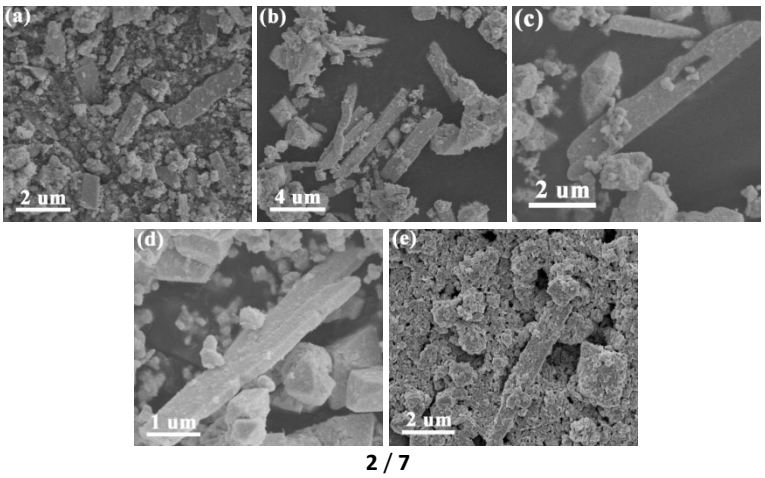

9

Fig. S1 SEM images of WP-4 at various reaction stages (a) 1h, (b) 3h, (c) 5h, (d) 8h, (e) 12h.

It can be seen from the Fig.S1 that with the extension of reaction time, the rod structure material shows a growth process, from the initial 2-3 um to 5-6 um. The rod-shaped sample is lead tungstate (it has been proved in the paper), and the nanoparticles on the surface of $PbWO_4$ are WO_3. In the process of reaction, the nanoparticle tungsten trioxide gradually compounds on the lead tungstate surface, forming a close contact phase interface.

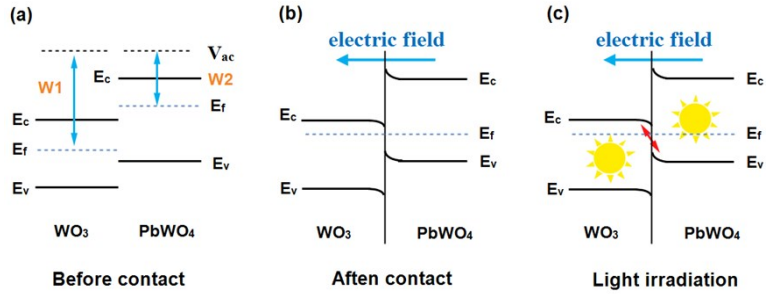

Fig. S2. (a) The band gap of WO_3 and $PbWO_4$. (b) The internal electric field and band edge bending at the interface of WO_3/$PbWO_4$. (c) The Z-scheme charge transfer mechanism between WO_3 and $PbWO_4$ under light irradiation

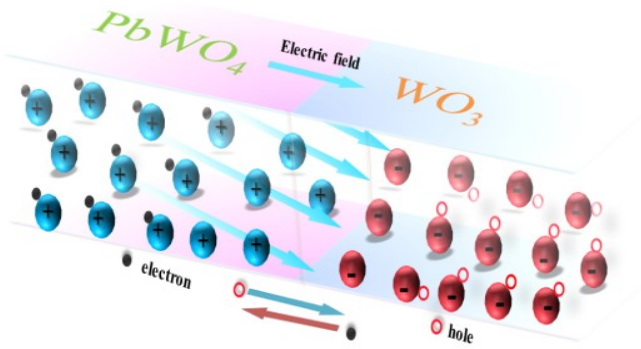

Fig. S3 The internal electric field

When semiconductors with different work function combined into a composite, electrons are migrated from one semiconductor to another, forming internal electric field (IEF) around the interface, which becomes the driving force of photogenerated carrier migration[8]. Recently, IEF engineering has emerged as an efficient method to improve photogenerated charge separation[9-11]. Scholars have found that interface interaction can enhance IEF[12-14]. Many composite photocatalysts have been demonstrated to construct IEF at heterogeneous interface. Such as, g-C_3N_4@Bi_2WO_6[15], CdS/BiOI/WO_3[16], WO_3/g-C_3N_4[17], CdS/WO_3[1], Bi_2WO_6/BiOI[18]. Therefore, when WO_3 and $PbWO_4$ are combined, IEF will be built due to different work function. WO_3 and $PbWO_4$ are both n-type semiconductor, the Fermi level of them is located near the CB of them. Based on the CB position

results of this work, it suggests the work function of WO_3 is higher than $PbWO_4$[19, 20]. The establishment process of the built-in electric field is described in Fig. S2. When $PbWO_4$ contacts with WO_3, electrons of $PbWO_4$ could transfer to WO_3 until reaching equilibrium, then band bending at grain boundary is established, and an IEF with $PbWO_4$ pointing to WO_3 is formed (Fig. S2b). Under light irradiation, IEF drives the photogenerated holes of $PbWO_4$ to move toward WO_3, while the photogenerated electrons of WO_3 move in the opposite direction, thus photogenerated carriers of WO_3 and $PbWO_4$ are separated according to the Z-type system (Fig. S2c).

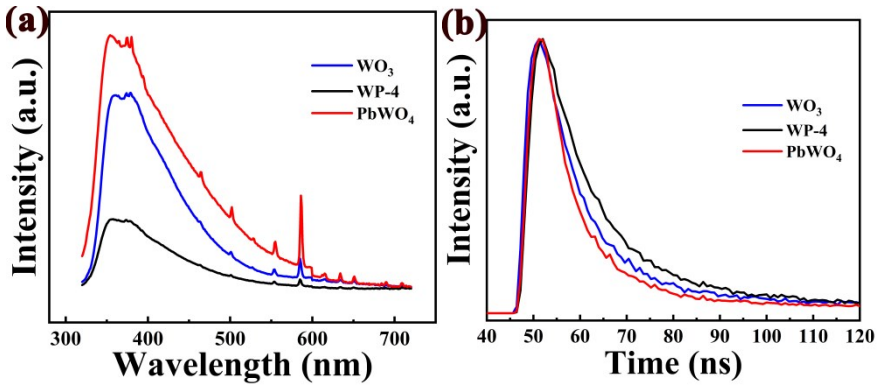

Fig. S4 (a) Steady-state PL spectra, (b) time-resolved transient PL decay of WO_3, $PbWO_4$ and WP-4

The steady-state photoluminescence (PL) spectrum reveals the carrier separation and transfers efficiency of the composites, as shown in Fig. S4a. It displays that the PL peak intensity of WP-4 is lower than WO_3 and $PbWO_4$, indicating that the recombination of photogeneration electron-hole pairs in WP-4 is forcefully suppressed due to the rapid separation of charge carrier across grain boundary. Moreover, the time-resolved photoluminescence spectroscopy (TRPL) is employed to elaborate on the specific charge carrier dynamics of WO_3, $PbWO_4$ and WP-4 (Fig.S4b). The fluorescent lifetime of PW-4 (10.3 ns) is larger than WO_3 (7.7 ns) and $PbWO_4$ (8.8 ns), indicating the photogenerated carriers of PW-4 need more times to decay than WO_3 and $PbWO_4$ after stopping illumination, which increases the possibility of photocarriers to participate in photo-oxidation reaction[21].

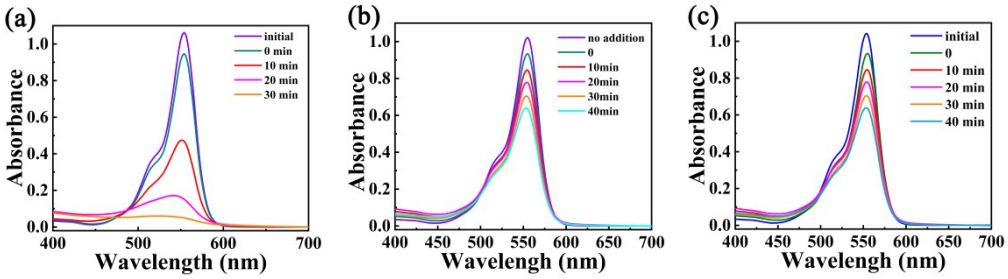

Fig. S5 UV-Vis absorption spectrum of PW-4 (a), UM (b), and PC (c)

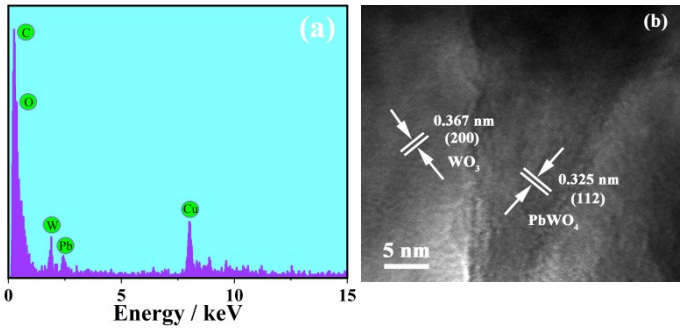

Fig. S6 (a) EDX spectra and (b) TEM with definite phase interface of the PC

According to the mass ratio of the WP-4, $PbWO_4/WO_3$ composite with interface is obtained according to *He, Hongcai's*[22] research. The EDX spectra and high-resolution TEM image of the physically contacted $WO_3/PbWO_4$ composite (PC) are measured to further prove that the combination of two similar crystal units can form a high-quality contact interface (Fig. S6 (a, b)). From Fig. S6b, a clear interface is observed, which is different from the TEM result of grain boundary with continuous phase transition. Due to PW-4 is connected by the same crystal structure unit, strong interaction exists between WO_3 and $PbWO_4$, and no gap between these two parts. As result, it is easier for photocarriers to transmit and separate in two parts.

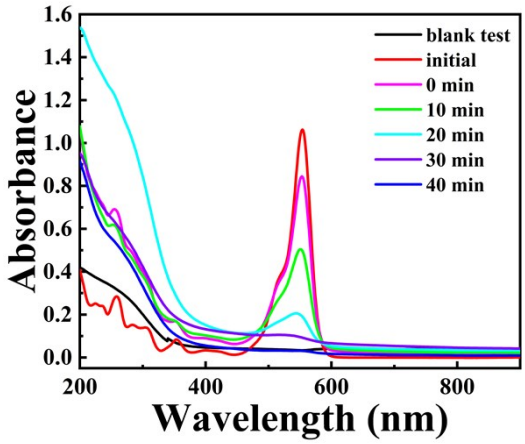

Fig. S7 UV-Vis absorption spectrum of PW-4

According to the UV-vis absorption spectra of RhB at different degradation time and the blank experiment (same condition but without RhB), as shown in Fig. S7. The slight blue shift of RhB maximum absorption wavelength is attributed to the N-deethylation of RhB. The main absorption peak disappears after 40 min, indicating the RhB molecule was thoroughly cracked. Carefully, the peaks below 400 nm disappear after 20 min, suggesting small aromatic ring compounds gradually disappear. The blank experiment result (the range of 300 nm - 200 nm), indicating the baseline will be raised

when using photocatalyst, which may be due to the small particles contained in centrifugal supernatant. The same phenomenon is also observed in the photocatalytic degradation experiment of RhB over PW-4. But the baseline is a little higher than a blank experiment, which may be due to some kinds of small molecules exist[23-26]. However, most RhB will be mineralized over PW-4 under illumination.

References

[1] L. J. Zhang, S. Li, B. K. Liu, D. J. Wang and T. F. Xie, ACS Catal, 2014, **4**, 3724-3729.

[2] S. Q. Zhang, T. Yu, H. Wen, R. Guo, J. J. Xu, R. X. Zhong, X. Li and J. H. You, RSC Adv., 2020, **10**, 16892-16903.

[3] G. Li, J. J. Hou, W. L. Zhang, P. W. Li, G. H. Liu, Y. G Wang and K. Y. Wang, Mater. Chem. Phys., 2020, **246**, 122827-122835.

[4] Chen D, Ye J. Hierarchical WO3Hollow Shells: Dendrite, Sphere, Dumbbell, and Their Photocatalytic Properties [J]. Advanced Functional Materials, 2008, **18**, 1922-1928.

[5] Z. F. Zhu, Y. Yan and J. Q. Li, Micro & Nano Letters, 2015, **10**, 460-464.

[6] D. Yue, W. Lu, M. N Wang, X. L. Zhang, Z. L. Wang and G. D. Qian. Rsc Adv., 2016, **6**, 81447–81453.

[7] R. Saraf, C. Shivakumara, S. Behera, H. Nagabhushana and N. Dhananjaya, S.A.P:M&B.S, 2015, **136**, 348-355.

[8] Y. Guo,W. X. Shi and Y. F. Zhu, EcoMat, 2019, **1**, 12007-12026.

[9] Y. Chen, W. Y. Yang, S. Gao, L. J. Zhu, C. X. Sun and Q. Li , ChemSusChem, 2018, **11**, 1521-1532.

[10] N. Esser and W. G. Schmidt, Phys. Status. Solidi. B, 2019, **256**, 1800314-1800319.

[11] J. Li, L. J. Cai, J. Shang, Y. Yu and L. Z. Zhang, Adv. mater., 2016, **28**, 4059-4064.

[12] X. J. Bai, C. P. Sun, S. L. Wu and Y. F. Zhu, J. Mater. Chem., 2015, **3**, 2741-2747.

[13] G. Z. Zhang, L. Yang, X. J. Wang, Z. Y. Wu, J. Jiang and Yi Luo, Adv. mater., 2018, **30**,1801988-1801917.

[14] X. P. Tao, Y. Y. Gao, S. Y. Wang, X. Y. Wang, Y. Liu, Y. Zhao, F. T. Fan, M. Dupuis, R. G. Li, and C. Li, Adv. Energy Mater, 2019, **9**, 1803951-1803957.

[15] Y. Y. Wang, W. J. Jiang, W. J. Luo, X. J. Chen and Y. F. Zhu, Appl. Catal. B, 2018, **237**,633-640.

[16] Q. Bia, Y. Gao, Z. Q. Wang, C. X. Dang, Z. K. Zhang, L. Wang and J. Q. Xue, Colloids and Surf. A, 2020, **599**, 124849-124860.

[17] J. W. Fu, Q. L. Xu, J. X. Low, C. J. Jiang, J. G. Yu, Appl. Catal. B, 2019, **243**, 556-565.

[18] X. Y. Kong, W. Q. Lee, A. R. Mohamed and S.P. Chai, Chem. Eng. J., 2019, **372**, 1183-1193.

[19] L. K. Putri, B. J. Ng, W. J. Ong, H. W. Lee, W. S. Chang and S. P. Chai, J. Mater. Chem. A, 2018, **6**, 3181-3194.

[20] R. Y. Wu, H. B. Song, N. Luo, Y. Sheng and G. J. Ji ,Solid State Sciences, 2019, **87**,101-109.

[21] F. He, G Chen, Y. G. Yu, S. Hao,Y. S. Zhou and Y. Zheng, ACS Appl. Mater. Interfaces, 2014, **6**, 7171−7179.

[22] Hongcai, Z. L. Jiang, Z. L. He, T. Liu, E. Z. Li and B. W. Li, Nano. Rese. Letters, 2018, **13**, 28-34.

[23] M. Yan, Y. L. Wu, Y. Yan, X. Yan, F. F. Zhu, Y. Q. Hua, and W. D. Shi, ACS Sustain. Chem. Eng., 2016, **4**, 757-766.

[24] J. Chen, X. Xiao, Y. Wang and Z. Ye, Appl. Surf. Sci. 2019, **467-768**, 1000-1010.

[25] K. Jothivenkatachalam, S. Prabhu, A. Nithya and K. Jeganathan, RSC Adv, 2014, **4**, 21221-21229.

[26] R. Y. Xie, K. J. Fang, Y. Liu, W. C. Chen, J. N. Fan, X. W. Wang, Y. F. Ren and Y. W. Song, J. Mater. Sci., 2020, **55**, 11919-11937.